

Tuning correlations in multi-component plasmas

Patrick Ludwig, Hauke Thomsen, Karsten Balzer, Alexei Filinov and Michael Bonitz

Institut für Theoretische Physik und Astrophysik Christian-Albrechts-Universität zu Kiel,
Leibnizstraße 15, 24098 Kiel, Germany

E-mail: ludwig@theo-physik.uni-kiel.de

Received 18 June 2010, in final form 26 July 2010

Published 15 November 2010

Online at stacks.iop.org/PPCF/52/124013

Abstract

Spontaneous, correlation-driven structure formation is one of the most fundamental collective processes in nature. In particular, particle ensembles in externally controlled confinement geometries allow for a systematic investigation of strong correlation and quantum effects over broad ranges of the relevant trap and plasma parameters. An exceptional feature inherent to finite systems is the governing role of symmetry and surface effects leading to similar collective behaviour in physical systems on vastly different length and energy scales. Considering (i) confined complex (dusty) plasmas and (ii) charge asymmetric bilayers, the effective range of the pair interaction emerges as a key quantity taking effect on the self-organized structure formation. Additional interest arises from the possible mass asymmetry of the plasma constituents in bilayers. Translating the results from (unconfined) 3D plasmas to bilayer systems, it is shown that the critical mass ratio required for crystallization of the heavy plasma component can be drastically reduced such that this effect becomes experimentally accessible.

(Some figures in this article are in colour only in the electronic version)

1. Introduction

Collective behaviour in many-particle systems with Coulomb interaction is a problem of high relevance in many fields of physics, chemistry, biology and beyond. Prominent examples are electrolytic solutions, dense plasmas, ultracold ions and atomic gases in traps, e.g. [1, 2], complex (dusty) plasmas [3–8], electrons and excitons in semiconductors [9–13] or folded small protein structures in biochemical systems [14]. It is remarkable that, despite the highly different nature and length scales of these systems, the occurrence of cooperative effects such

as structure formation or collective dynamic properties is captured by just two dimensionless parameters, which measure the ratio of the mean interaction energy E_{int} to the average kinetic energy E_{kin} in the system,

$$\Gamma \equiv \frac{Q^2}{a k_B T} \quad r_s \equiv \frac{a}{a_B} \sim Q^2 m a. \quad (1)$$

Here, Γ is the coupling parameter of a classical Coulomb system with charge Q and mean interparticle distance $a \sim n^{-D}$ (n is the system density and $D = 1, 2, 3$ its dimensionality). In quantum systems Γ is replaced by the Brueckner parameter r_s [15] which does not involve temperature T but the Bohr radius, $a_B = 4\pi\epsilon\hbar^2/(mQ^2)$. In traditional plasmas E_{int} is small compared with E_{kin} . In contrast, when Γ (or r_s) exceed unity, correlation effects start to dominate the plasma behaviour giving rise to spatial ordering. In particular, when $\Gamma \gtrsim 100$ (or $r_s \gtrsim 100$) crystal-like ordering emerges as was observed in trapped ions or dusty plasmas. The behaviour of these plasma crystals was studied in great detail over the last two decades, see, e.g. [16] for a recent overview.

Here we are interested in the question to what degree the correlated plasma behaviour and crystallization, in particular, can be externally controlled. We consider two examples. The first are spherical crystals in dusty plasmas ('Yukawa balls') and the second is a two-component plasma in two spatially separated layers. While in the former, control can be achieved via an external trapping potential and the surrounding plasma (screening strength), in the latter case, an additional control is offered by the layer separation and the choice of the semiconductor material which allows us to control the mass ratio of the two charge species.

2. Controlling plasma crystallization in traps

As an example of spatially confined plasma crystals we consider Yukawa balls [5] which consist of concentric crystal shells strongly resembling trapped ion crystals, e.g. [1, 6], with the key difference that the pair interaction between the particles forming the crystal is screened by the electrons and ions of the ambient plasma [7]. Despite screening, in a dusty plasma the range of strong coupling is extended to temperatures many orders higher since the individual particles are not singly but highly charged. In fact, according to equation (1), by increasing the individual dust grain charges to $Q = 1000e \dots 10\,000e$ the repulsive interaction amongst these plasma constituents can be tuned such that plasma crystallization becomes observable even under room temperature conditions. The Hamilton function of N identical dust particles reads as

$$H = \sum_{i=1}^N \frac{p_i^2}{2m} + \sum_{j>i}^N \frac{Q^2 e^{-\kappa|r_i - r_j|}}{4\pi\epsilon|r_i - r_j|} + \sum_{i=1}^N U(r_i), \quad (2)$$

where r_i denotes the coordinate of the i th particle. In the experiments of Arp *et al* [5] ion flow and wake effects were found to be negligible whereas the total confinement potential produced by electrostatic potentials, thermophoresis and gravity is well approximated by an isotropic parabolic potential (which is assumed to be independent of screening), $U(r_i) = m\omega_0^2 r_i^2/2$ [17]. Comparison with molecular dynamics (MD) simulations [7] allowed to verify that this model captures the dominant properties of the Yukawa balls: as in the experiment, the dust particles form concentric shells which are almost equally spaced, and even the shell populations could be well reproduced by model (2). This is seen in the left part of figure 1 which shows the shell populations for 43 experimentally observed Yukawa balls and molecular dynamics

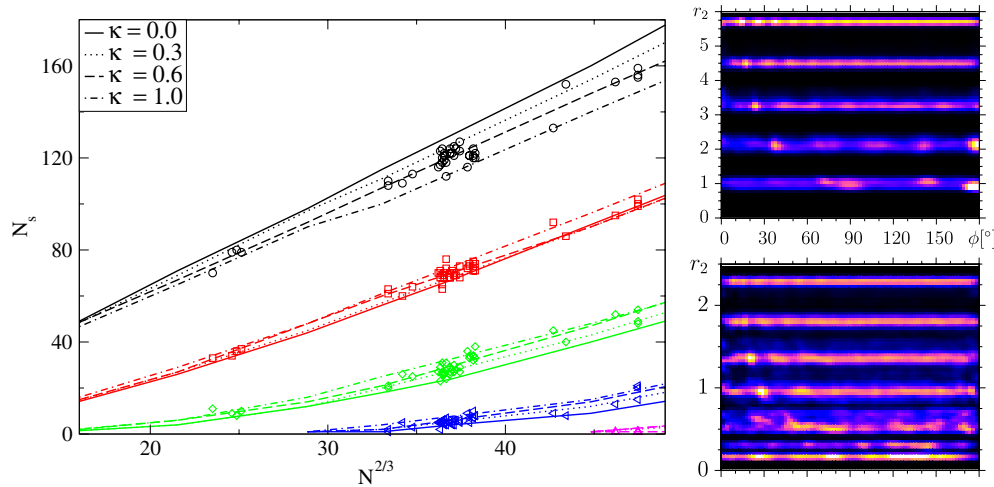


Figure 1. Left: experimental (symbols) and simulation (lines) shell populations N_s of harmonically confined dust crystals as a function of the system size $N^{2/3}$. The simulation results (lines) are obtained for different screening parameter κ and show that the particles are redistributed from the outer shell to inner shells with increased screening. From [7]. Right: three particle correlation function for 3D plasma crystals with $N = 500$, $\Gamma = 1000$, and screening parameter $\kappa = 0$ (top) and $\kappa = 3.8$ (bottom). White (black) denotes areas of high (low) correlation; r_1 is integrated out.

simulation results for several values of the Debye screening parameter κ (which is the only free parameter in the simulations).

The most remarkable finding is a high sensitivity of the shell occupation numbers to the precise value of κ (range of the interaction potential). A screened interaction changes the structure of the cluster such that the occupation numbers on the inner (outer) shells gradually increase (decrease). This implies that a Yukawa system contains a smaller (or equal) number of particles on the outer and a higher (or equal) number of particles on the inner shell than an unscreened Coulomb system with the same N . Therefore, the structural fingerprint allows for a novel non-invasive diagnostic to determine the Debye screening length on the basis of the observed shell occupation numbers measured in experiments. Best agreement with the measurements is found for $\kappa r_0 \approx 0.6$ ¹ which agrees well with independent estimations [18]. The reason for the change in the shell population number is a screening-induced radial density gradient, which leads to a (with κ increasing) density decay toward the cluster surface to establish a (local) force equilibrium [19, 20].

The formation of distinct shells is a typical finite-size effect reflecting the geometrical constraints of the external confinement, which leads to a striking sensitivity with regard to the *exact* particle number N . By simply adding or removing a single-particle qualitative transformations of the collective interplay can be achieved, resulting in drastically different physical properties [9, 21]. In allusion to the periodic table of the chemical elements, periodic Mendeleev-type tables have been extensively studied, in particular for parabolically confined Coulomb [6, 22] and Yukawa [3, 23] systems.

Approaching large cluster sizes the dependence on the precise particle number vanishes, the shells break up and finally regular volume order prevails [24, 25]. In the right part of

¹ Sources of errors such as fluctuations of charge and temperature were found to be small [28] and also the occurrence of metastable states in the experiments has a negligible influence on this result.

figure 1 we present first results of the *three particle correlation function* (TPCF)², which gives direct insight into the internal structure of a Yukawa ($\kappa = 3.8$) and a Coulomb ($\kappa = 0$) cluster of intermediate size $N = 500$ and $\Gamma = 1000$. Comparing both systems, the first observation is that the reduced repulsion for $\kappa > 0$ leads to a strong compression of the entire cluster. In the Coulomb case we find five distinct shells. Due to the quadratic increase in the confinement strength in the radial direction the (thermal) delocalization on the cluster surface is strongly reduced. Seven (almost oppositely arranged) particles in the innermost shell result a strong peak close to 180° . Also the other four shells show several sharp peaks that reflect the high internal symmetry of the Coulomb cluster. Upon increase in κ , the screened interaction becomes short-ranged and the TPCF reveals the strong competition between bulk and spherical order. While in the outer region of the Yukawa cluster a pronounced shell structure remains, in the cluster core (where the influence of the external confinement is weaker) the emergence of several close sub-shells is observed, which marks the appearance of a bulk-like (close-packed) symmetry. The formation of bcc order in the bulk of Coulomb crystals is expected to begin for systems with $N \gtrsim 10^4$ particles [25].

It should be noted that a change in the effective range of the interaction potential has not only influence on the structural properties [23], but was also found to have a direct impact on the dynamical and spectral features [16, 21, 26] as well as on the cluster melting behaviour [8, 27].

3. Correlation control in charge asymmetric bilayers

Bilayers containing spatially separated negative (e) and positive (h) charge carriers are an utmost versatile two-component system, standing in between neutral and non-neutral Coulomb systems on the one hand, and between two-dimensional and three-dimensional systems on the other. Possible realizations include electron–ion plasmas and electron–hole systems in semiconductors. Quantum bilayers can be realized by separating electrons and holes in two coupled (well insulated) quantum wells (QWs) or in a single QW where charge separation is achieved by applying a strong electric field perpendicular to the well plane [29]. A fascinating property of e–h quantum bilayers arises from the additional control of correlation effects by (a) varying the separation d and (b) by the choice of the two components.

- (a) Variation of d allows for a continuous transition from (starting from large d): (i) two weakly coupled Coulomb layers to an effective single layer system [21], (ii) free particles to e–h bound states (indirect excitons) with an effective dipole–dipole interaction and (iii) Fermi statistics to Bose statistics (composite bosons). This will be discussed in section 3.1.
- (b) In a two-component plasma an additional degree of freedom is provided by the charge ratio and the mass ratio of the components which have a strong influence on the observed phases [30]. Here we concentrate on the effect of the mass ratio $M = m_h/m_e$ assuming symmetric charges $-q_e = q_h$. Variation of M allows us to tune the relative importance of quantum effects in both components via the thermal DeBroglie wavelength $\Lambda_a = h[2\pi m_a k_B T]^{-1/2}$, $a = e, h$. At the same time the strength of correlations in the two components is modified via the coupling parameter r_{s_a} . This will be discussed in section 3.2.

In the following we will discuss the control of correlations in bilayer systems, in particular in view of crystallization phenomena, by these two parameters.

² The TPCF gives the probability of an arbitrary particle in the cluster to ‘see’ another particle at position (r_2, ϕ) with respect to the trap centre (in spherical coordinates). While the name TPCF follows the definition in extended macroscopic systems, here we use the trap centre instead of a third particle as the third reference point to take into account the symmetry of the confined system.

3.1. Strongly correlated indirect excitons in quantum wells

The possibility of confinement and manipulation of excitons in potential traps has attracted considerable interest in the last two decades because these systems are expected to exhibit collective quantum phenomena such as Bose–Einstein condensation and superfluidity, e.g. [10, 13]. A suitable electrode geometry which separates the charge carriers³ and at the same time creates a parabolic confinement for the neutral excitons within the QW plane can be generated by a fine tip electrode due to the *quantum-confined Stark effect* [29]. This permits for a voltage-controlled transition from the direct to the spatially indirect exciton (IE) regime providing high flexibility in manipulating and controlling the exciton parameters: tuning the applied voltage and the electrode to sample distance the depth and the steepness of the in-plane confinement can be independently changed. This allows us to reach very high exciton densities which in combination with the induced repulsive dipole moment brings the IEs to a strongly correlated state.

For a first principle description of IEs in the moderate (bosonic) density regime at finite temperature we use path integral Monte Carlo (PIMC) simulations⁴. The considered N -particle Hamiltonian,

$$\hat{H} = \hat{H}_e + \hat{H}_h + \sum_{j>i}^N \frac{e^2}{4\pi\epsilon\sqrt{(\mathbf{r}_i - \mathbf{r}_j)^2 + (z_i - z_j)^2}}, \quad (3)$$

captures all Coulomb interaction contributions without simplification. The $N = N_e + N_h$ single-particle contributions are given by

$$\hat{H}_{e(h)} = \sum_{i=1}^{N_{e(h)}} \left(-\frac{\hbar^2}{2m_{e(h)}^*} \nabla_{\mathbf{r}_i}^2 + \frac{m_{e(h)}^*}{2} \omega_0^2 \mathbf{r}_i^2 + U_{e(h)} \right), \quad (4)$$

which include the kinetic (band) energy, the harmonic in-plane confinement with the effective trap frequency ω_0 and an additional external potential $U_{e(h)}$, which combines the effect of the QW confinement (presented as a square well) and the applied electric field⁵. In the simulations we use a fixed mass ratio, corresponding to realistic electron (hole) masses $m_{e(h)}^*$ [29].

Figure 2 represents typical IE density distributions obtained in the simulations and demonstrates a temperature-driven crystallization of excitons (the average density is $n = 1.5 \times 10^{10} \text{ cm}^{-2}$): at $T = 3.35 \text{ K}$, the IEs are in a gas state and delocalized within the trap due to thermal fluctuations. (i) By lowering temperature to 830 mK, the excitons become strongly correlated and enter a *radially ordered quantum state*. Due to the concentric shape of the confinement, the $N_x = 56$ IEs arrange themselves on four shells. (ii) Further lowering of temperature to 210 mK leads to a full freeze-out of the thermal fluctuations, only (zero-point) quantum fluctuations prevail. The repulsive inter-exciton interaction is capable of governing the strong quantum fluctuations and establishes a localization of excitons within the shells. The PIMC results clearly reveal the existence of a bosonic Wigner nano-crystal with a *regular hexagonal 2D Wigner lattice* in the trap centre (where the geometrical constraints of the external confinement are reduced). The distinct peaks in the diffraction patterns, obtained from the

³ The main issue of excitons is their finite lifetime. One possibility to considerably lower the spontaneous recombination probability of excitons is to reduce the e–h wave function overlap by spatial separation of electrons and holes [31].

⁴ For implementation details and further references see [20].

⁵ The considered effective e–h pair separation of $d = 20 \text{ nm}$ ($6.6a_B$) can be produced by an electric field of strength $E_z = 20 \text{ kV cm}^{-1}$ in a single ZnSe-based quantum well of $L = 30 \text{ nm}$ width [29].

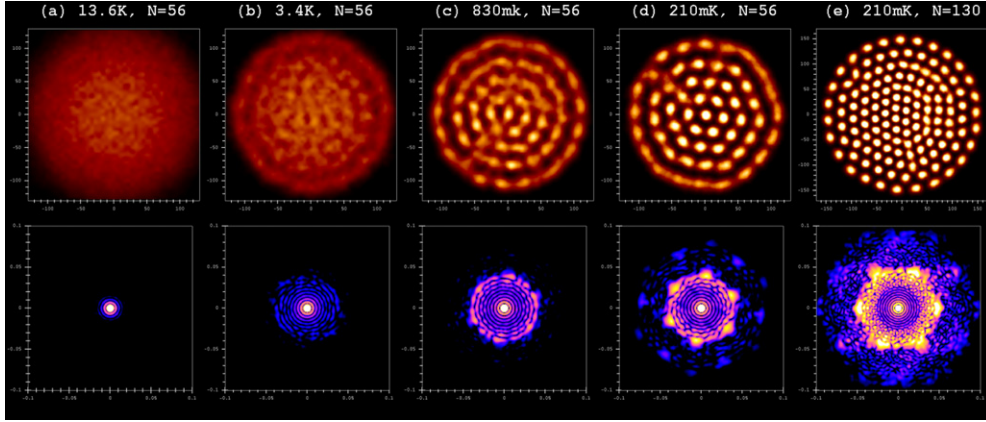


Figure 2. Temperature-driven phase transition of (a)–(d) $N_x = 56$, (e) $N_x = 130$ harmonically trapped indirect excitons in a 30 nm wide ZnSe-based quantum well. Top row: density plots for the temperatures: 13.6 K, 3.4 K, 830 mK and 210 mK (from left to right). Due to strong inter-exciton correlations highly ordered quantum states, including a bosonic Wigner nano-crystal, are observed. Partial exciton delocalization is a result of quantum fluctuations and Bose statistics (‘cold’ melting). Plotted area: $A = 130 \times 130 a_B^2$ [(e) $170 \times 170 a_B^2$]. Bottom row: corresponding Bragg diffraction patterns exhibiting the degree of order in a system by measuring the density–density correlations. The patterns give a clear evidence for a phase transition in the mesoscopic system. (Diffraction intensity is logarithmically scaled.)

spatial 2D Fourier transform of the time averaged exciton density distribution $n(r)$, give a clear evidence for a phase transition in this mesoscopic system⁶ [33].

The observed two-stage transition process is a well-known phenomenon in confined (classical as well as quantum) few-particle systems, e.g. [8, 9, 12]. This is due to the fact that the confinement induced radial energy barriers are considerably higher than the intrashell energy barriers separating the repelling particles. Because of the short range of the dipole potential, the mesoscopic quantum crystal of IE appears at higher densities than the electron (Coulomb) Wigner crystal, i.e. the crystal is stabilized. The literature value for the transition from the Fermi liquid state to the *electron* Wigner crystal phase is $r_s^e \approx 35$ [9, 12], whereas the crystal of *dipolar excitons* is already found at $r_s^x \approx 25$.

It should be noted that such crystalline islands in parabolic traps can exist only in small systems with $N_x \leq 10^3$. The reason is an inhomogeneous density profile, which is caused by the short range character of the dipole potential (a similar effect is observed for Yukawa balls, see section 2). Hence, the increase in N_x results in an increasing exciton density in the trap centre. The 2D exciton crystal is found to exist only in a narrow density interval, $n_1 \leq n \leq n_2$ [10, 11]. Thus we expect to observe crystalline structures in a typical experiment with a macroscopic number of excitons only in a certain region of the trap, where the local density $n(r)$ matches the condition: $n_1 \leq n(r) \leq n_2$.

In figure 3 we present self-consistent Hartree–Fock (HF) ground state results for two coupled layers of spin-polarized (fermionic) electrons and holes⁷. It is shown how an ideal trapped quantum system ($d = 0$) evolves to a strongly coupled one if the layer separation d is increased, i.e. an effective dipole–dipole repulsion is turned on. Then, the mutual interplay of attractive interlayer and repulsive intralayer Coulomb forces leads to a localization of

⁶ The classification follows the *International Union of Crystallography* (IUC) which redefined the term ‘crystal’ to mean ‘any solid having an essentially discrete diffraction diagram’ in 1991 [32].

⁷ For implementation details of the applied Hartree–Fock method see [20, 21].

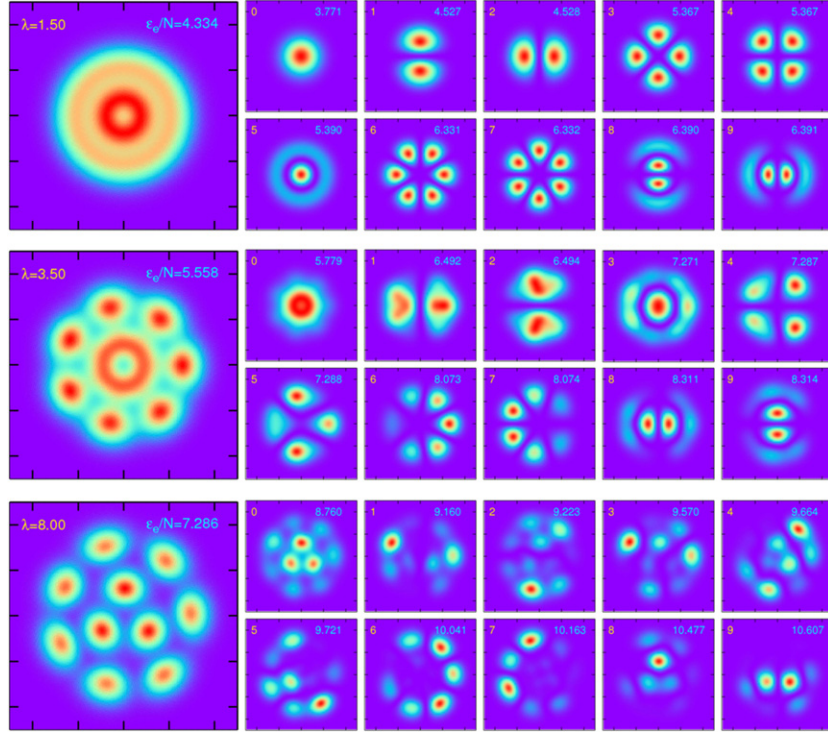


Figure 3. Hartree–Fock ground states of $N_{e(h)} = 10$ electrons and holes in a coupled (mass symmetric) bilayer system indicating a phase transition from a Fermi liquid to strongly coupled state upon increase in e–h separation $d = \lambda \times 12\pi\epsilon\hbar^2 / (e^2 m_{e(h)})$ and $\lambda = 1.5, 3.5$, and 8.0 (from top to bottom). Left: accumulated N -particle density $\rho^{e(h)}(\mathbf{r})$. Right: corresponding densities of the 10 energetically lowest single-particle orbitals $\rho_i^{e(h)}(\mathbf{r})$ (identical for electrons and holes). Note that the 10 high-density spots of the N -particle density for $\lambda = 8$ do not necessarily correspond to the single particles themselves as the configuration appears as a superposition of all orbitals.

states and an essential stabilization of the many-particle quantum system. Moreover, the HF results clearly demonstrate that, even in the Wigner crystal phase where the density shows strong peaks, the single density peaks do not necessarily correspond one-to-one to single particles, but rather the single-particle orbitals extend over the entire cluster. This means with respect to the exciton Wigner crystal that the identification of single excitons (individual exciton wave packets) is not obvious and may lead to misinterpretations due to ‘matter wave overlap’ [21].

3.2. Hole Wigner crystallization in mass-asymmetric e–h bilayers

In the following we concentrate on the second parameter in question which (besides temperature, density and layer separation) has a significant influence on many-particle correlation effects in e–h bilayers: the effective mass ratio $M = m_h/m_e$. As was recently predicted for a bulk semiconductor, holes undergo a phase transition to a crystalline state if the mass ratio exceeds a critical value of $M_{cr} = 80$ [30]. At the same time the electrons are—due to their smaller mass—strongly degenerate and form a Fermi gas or liquid. However, this high value of M_{cr} complicates the search for experimental evidence of the hole Wigner crystal

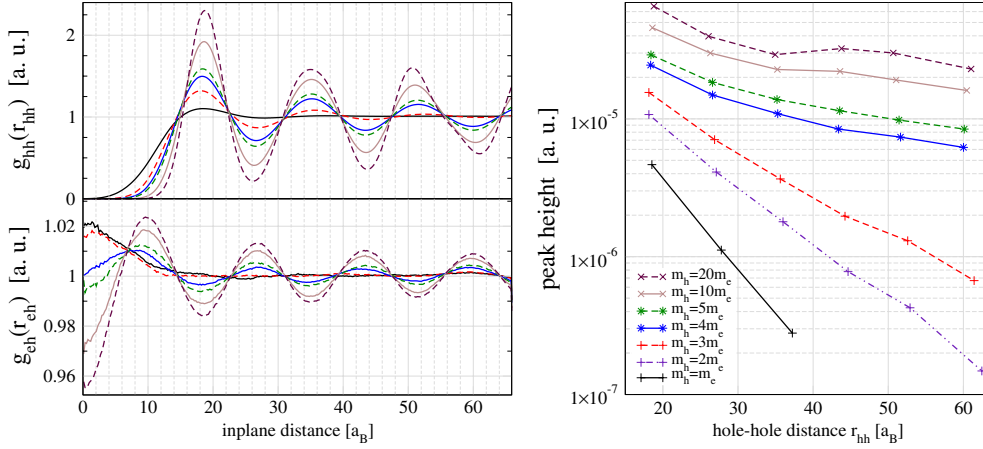


Figure 4. Left: hole–hole (top) and e–h (bottom) pair distribution functions for a macroscopic bilayer with the mass ratios $M = 1, 3, 4, 5, 10, 20$ (the maxima increase with increasing M). Note the alternating location of maxima and minima of g_{hh} and g_{eh} . Right: decay of the amplitude of the maxima and minima of the hole correlations ($|g_{hh} - 1|$) for the seven mass ratios. From [34].

since the e–h mass ratio of a typical semiconductor is on the order of 10^8 . For this reason, it is interesting to analyze the effect of the mass ratio M_{cr} on hole crystal formation in an e–h bilayer system, where M_{cr} depends on the layer separation d . The layer separation $d = 20a_B$ is chosen such that the *repulsive intralayer interaction* and *attractive interlayer interaction* are on the same energy scale, i.e. the system shows real 3D behaviour. The complicated overlap of Coulomb interactions and quantum effects of both, electrons and holes, are treated on first principles by PIMC methods [34].

In figure 4 (left part) we show the hole–hole pair distributions g_{hh} for a macroscopic bilayer system with periodic boundary conditions at low temperature where thermal effects are negligible. The mass ratio M is varied between 1 and 20. Since the average particle density is constant (the in-plane density parameter is $r_s = 10$), the position of the first peak of g_{hh} is practically independent of M . In contrast, the general behaviour of g_{hh} changes significantly: for $M \geq 4$ there are clear oscillations typical for the solid phase. Even the third and fourth peaks are well resolved. These oscillations become rapidly damped by reducing M to 3 and below, here g_{hh} shows liquid-like features.

The effect of the interlayer correlations for the stability of the hole crystal is apparent from the e–h pair distribution g_{eh} (see bottom left part of figure 4). For the symmetric case, $M = 1$, and also for $M = 3$ the electrons reside with the highest probability just below the holes. The modulation depth is around 2% only because of the high electron degeneracy (delocalization). This means that these peaks cannot be associated with bound states (indirect excitons) since the electron density is well above the Mott density n_{Mott} where excitons break up. For larger mass ratios, $M \geq 4$, a completely different behaviour of g_{eh} emerges. Now, the maximum of g_{eh} vanishes at zero distance, and the function exhibits oscillations. The electron density is modulated due to the presence of the hole crystal with maxima located in between the holes which become systematically more pronounced when M increases. The (dis-)appearance of these oscillations of g_{eh} indicates a phase transition in the asymmetric bilayer system which is more clearly seen in g_{hh} .

⁸ A further issue is the relatively short radiative lifetime in the case that the e–h wavefunctions are not spatially separated as in the case of indirect excitons, see section 3.1.

The peak height (amplitude) of g_{hh} as a function of the peak position r_{hh} (figure 4, right part) clearly shows a change in the correlation decay law with M . The change from a ‘liquid’ state with *exponential correlation decay* (for $M \leq 3$) to a *power law decay* (for $M \geq 4$) signals a Kosterlitz–Thouless transition to a quasi-long range order (solid-like). Hence, the critical mass ratio at which quantum melting of the hole crystal takes place is around $M_{cr} \approx 3.5$ and is much smaller than the value of $M_{cr} \approx 80$ in a 3D bulk system [30]. This result underlines the remarkable additional control of correlation phenomena in a bilayer system by variation of the layer separation d . An experimental observation of hole crystallization with standard semiconductor materials should be feasible.

4. Conclusions

In this paper we have discussed Coulomb crystallization in strongly correlated plasmas. Considering two examples (i) Yukawa balls in dusty plasma and (ii) charge asymmetric bilayers, our special interest was devoted to the possibilities to externally control plasma crystallization. In the former, we have addressed the question of how Debye shielding and finite-size effects influence the structural properties of these systems. In the second example, we have shown that there exist two independent ways to control crystallization: via variation of d (exciton crystallization) and via variation of the mass ratio M (hole crystallization). While we have not covered the whole phase diagram, it is clear from these examples that there exists a rich variety of ways to control correlation phenomena. Due to the high scalability of Coulomb systems, we expect that these results will also be of interest to other types of strongly coupled multi-component plasmas.

Acknowledgments

PL acknowledges fruitful discussions with Gabor Kalman. This work was supported by the Deutsche Forschungsgemeinschaft via SFB-TR24 and grant LU 1586/1-1.

References

- [1] Itano W M *et al* 1998 *Science* **279** 686
- [2] Mortensen A *et al* 2006 *Phys. Rev. Lett.* **96** 103001
- [3] Juan W-T *et al* 1999 *Chin. J. Phys.* **73** 184
- [4] Melzer A 2003 *Phys. Rev. E* **67** 016411
- [5] Arp O *et al* 2004 *Phys. Rev. Lett.* **93** 165004
- [6] Ludwig P *et al* 2005 *Phys. Rev. E* **71** 046403
- [7] Bonitz M *et al* 2006 *Phys. Rev. Lett.* **96** 075001
- [8] Ogawa T *et al* 2006 *J. Phys. Soc. Japan* **75** 123501
- [9] Filinov A *et al* 2001 *Phys. Rev. Lett.* **86** 3851
- [10] De Palo S *et al* 2002 *Phys. Rev. Lett.* **88** 206401
- [11] Filinov A *et al* 2003 *Phys. Status Solidi c* **0** 1518
- [12] Ghosal A *et al* 2006 *Nature Phys.* **2** 336
- [13] Timofeev V B and Gorbunov A V 2007 *J. Appl. Phys.* **101** 081708
- [14] Zhang F *et al* 2008 *Phys. Rev. Lett.* **101** 148101
- [15] Bonitz M *et al* 2008 *Phys. Plasmas* **15** 055704
- [16] Bonitz M *et al* 2010 *Rep. Prog. Phys.* **73** 066501
- [17] Arp O *et al* 2005 *Phys. Plasmas* **12** 122102
- [18] Block D *et al* 2008 *Phys. Plasmas* **15** 040701
- [19] Henning C *et al* 2006 *Phys. Rev. E* **74** 056403
Henning C *et al* 2007 *Phys. Rev. E* **76** 036404

- [20] Bonitz M, Horing N and Ludwig P (ed) 2010 *Introduction to Complex Plasmas* (Springer Series: Atomic, Optical and Plasma Physics) (Berlin: Springer)
- [21] Ludwig P *et al* 2008 *New J. Phys.* **10** 083031
- [22] Kong M *et al* 2002 *Phys. Rev. E* **65** 046602
- [23] Baumgartner H *et al* 2008 *New J. Phys.* **10** 093019
- [24] Schiffer J 2002 *Phys. Rev. Lett.* **88** 205003
- [25] Totsuji H *et al* 2002 *Phys. Rev. Lett.* **88** 125002
- [26] Henning C *et al* 2008 *Phys. Rev. Lett.* **101** 045002
- [27] Apolinario S W S and Peeters F M 2007 *Phys. Rev. E* **76** 031107
- [28] Baumgartner H *et al* 2007 *Contrib. Plasma Phys.* **47** 281
- [29] Ludwig P *et al* 2006 *Phys. Status Solidi b* **243** 2363
- [30] Bonitz M *et al* 2005 *Phys. Rev. Lett.* **95** 235006
Bonitz M *et al* 2006 *J. Phys. A: Math. Gen.* **39** 4717
- [31] Ludwig P 2008 *PhD Thesis* Universität Rostock
- [32] 1992 *Foundations of Crystallography* IUCr: Report of the Executive Committee for 1991 *Acta Crystallogr. A* **48** 922
- [33] Sperlich K *et al* 2009 *Phys. Status Solidi c* **6** 551
- [34] Ludwig P *et al* 2007 *Contrib. Plasma Phys.* **47** 335